

Microstructure and velocity of field-driven Ising interfaces moving under a soft stochastic dynamic

Per Arne Rikvold^{1,2,*} and M. Kolesik^{3,4,†}

¹*Center for Materials Research and Technology, School of Computational Science and Information Technology, and Department of Physics, Florida State University, Tallahassee, Florida 32306-4350*

²*Center for Stochastic Processes in Science and Engineering, Department of Physics, Virginia Polytechnic Institute and State University, Blacksburg, VA 24061-0435*

³*Institute of Physics, Slovak Academy of Sciences, Bratislava, Slovak Republic*

⁴*Optical Sciences Center, University of Arizona, Tucson, Arizona 85721*

(Dated: November 20, 2018)

We present theoretical and dynamic Monte Carlo simulation results for the mobility and microscopic structure of 1+1-dimensional Ising interfaces moving far from equilibrium in an applied field under a single-spin-flip “soft” stochastic dynamic. The soft dynamic is characterized by the property that the effects of changes in field energy and interaction energy factorize in the transition rate, in contrast to the nonfactorizing nature of the traditional Glauber and Metropolis rates (“hard” dynamics). This work extends our previous studies of the Ising model with a hard dynamic and the unrestricted SOS model with soft and hard dynamics. [P. A. Rikvold and M. Kolesik, *J. Stat. Phys.* **100**, 377 (2000); *J. Phys. A* **35**, L117 (2002); *Phys. Rev. E* **66**, 066116 (2002).] The Ising model with soft dynamics is found to have closely similar properties to the SOS model with the same dynamic. In particular, the local interface width does *not* diverge with increasing field, as it does for hard dynamics. The skewness of the interface at nonzero field is very weak and has the opposite sign of that obtained with hard dynamics.

PACS numbers: 05.10.ln 68.35.Ct 75.60.Jk 68.43.Jk

*Electronic address: rikvold@csit.fsu.edu

†Electronic address: kolesik@acms.arizona.edu

I. INTRODUCTION

The structure and dynamics of surfaces and interfaces significantly influence a host of material properties. Consequently, an enormous amount of work has been devoted to the study of moving and growing interfaces [1, 2]. However, despite the fact that many important interface properties, such as mobility and chemical activity, are largely determined by the *microscopic* interface structure, the bulk of this effort has concentrated on large-scale scaling properties.

Since the detailed physical mechanisms of the interface motion are most often unknown, it is useful to model the dynamic as a stochastic process defined by a set of transition probabilities. It is therefore important to gain better insight into how the driving force (such as an applied magnetic or electric field or a chemical-potential difference) may alter the microscopic interface structure for different stochastic dynamics. Recently we have studied the influence of the stochastic dynamics on the microscopic structure and mobility of Ising and solid-on-solid (SOS) interfaces that move under two types of Glauber dynamics [3, 4, 5]. Both Ising and SOS interfaces are described by the Ising Hamiltonian

$$\mathcal{H} = - \sum_{x,y} s_{x,y} (J_x s_{x+1,y} + J_y s_{x,y+1} + H) , \quad (1)$$

where $s_{x,y} = \pm 1$ is an Ising spin at lattice site (x, y) , $\sum_{x,y}$ runs over all sites on a square lattice, and J_x and J_y are ferromagnetic interactions in the x - and y -directions, respectively. The quantity H is the applied “field,” and the interface is introduced by fixing $s_{x,y} = +1$ and -1 for large negative and positive y , respectively. We take $H \geq 0$, such that the interface on average moves in the positive y direction. (This model is equivalent to a lattice-gas model with local occupation variables $c_{x,y} \in \{0, 1\}$, see details in Ref. [5].) The difference between the two interface types is that the Ising interface allows overhangs and bubbles, while these are forbidden in the SOS interface. However, at low and intermediate temperatures overhangs and bubbles in an Ising interface are rare, and a short interface segment is likely to be indistinguishable from an SOS interface. A typical SOS interface is illustrated in Fig. 1.

In addition to bubbles that are generated *at* the interface by pinching off of protrusions or indentations, Ising models in an applied field can also contain bubbles created by homogeneous nucleation in the bulk phases [6, 7, 8]. While such bubbles destroy the integrity of the interface at very strong fields, they have only a minor influence on the mobility at moderate fields [7, 8]. In this paper, like in Ref. [3], we exclude such nucleated bubbles by setting the transition rate equal to zero for sites that have no neighbors with the opposite spin direction. As a consequence, the bulk phases far from the interface are uniform.

The interface dynamic is defined by the set of single-spin transition probabilities, $W(s_{x,y} \rightarrow -s_{x,y})$, and time is

measured in units of attempted MC updates per site (MC steps per site, or MCSS). The first one of the dynamics used in the aforementioned studies [3, 4] is the standard discrete-time Glauber dynamic with the transition probability [9]

$$W_G(s_{x,y} \rightarrow -s_{x,y}) = [1 + e^{\beta\Delta E}]^{-1}, \quad (2)$$

where ΔE is the total energy change that would result from the transition. Although ΔE can be written as a sum of the energy change ΔE_J , due to the change in the interaction part of the Hamiltonian, and ΔE_H , due to the change in the field energy, this transition rate itself cannot be factorized into a product of parts that depend only on ΔE_J and ΔE_H , respectively. This dynamic is therefore classified as “hard” in the literature on driven particle systems [10].

The second type of dynamics is defined by transition probabilities that factorize into a part that depends only on ΔE_J and one that depends only on ΔE_H . Such dynamics are known as “soft” [10]. In our recent study of a driven SOS interface with soft dynamics we used, for reasons of mathematical convenience, the “soft Glauber dynamic” [4] in which each of the two parts has the Glauber form:

$$W_{SG}(s_{x,y} \rightarrow -s_{x,y}) = [1 + e^{\beta\Delta E_H}]^{-1} \cdot [1 + e^{\beta\Delta E_J}]^{-1}. \quad (3)$$

Soft dynamics (usually with the field part proportional to a Metropolis transition rate [11, 12]) are often used for lattice-gas simulations, in which the field term corresponds to the entropic part of a chemical-potential difference. In Ref. [4] we showed, in agreement with a theoretical prediction in Ref. [3], that the soft dynamic leads to a microscopic SOS interface structure that is identical to the equilibrium interface in zero field, irrespective of the value of the applied field. This is in contrast with the result for hard dynamics [5], which lead to an intrinsic interface width that increases dramatically with the field. The purpose of the present paper is to study the effects of the soft Glauber dynamic for an Ising interface (which may contain bubbles and overhangs) and compare those with the cases of an Ising interface with the standard (hard) Glauber dynamic [3] and SOS interfaces with the soft Glauber dynamic [4] and hard Glauber dynamic [5].

The rest of this paper is organized as follows. Theoretical results for the interface structure and velocity are surveyed in Sec. II. Comparisons with extensive dynamic MC simulations are given in Sec. III, with results for the interface velocity in Sec. III A and for the interface structure and skewness in Sec. III B. Our conclusions are drawn in Sec. IV.

II. INTERFACE STRUCTURE AND VELOCITY

With the Ising Hamiltonian there is only a finite number of different values of ΔE , and the spins can therefore be divided into classes [13, 14, 15], labeled by the spin value s and the number of broken bonds between the spin and its

nearest neighbors in the x and y direction, j and k , respectively. The eighteen different Ising spin classes are denoted jks with $j, k \in \{0, 1, 2\}$. They are listed in Table I, and subsets are also listed in Table II and shown in Fig. 1.

The Burton-Cabrera-Frank SOS model [16] considers an interface in a lattice gas or $S = 1/2$ Ising system on a square lattice of unit lattice constant as a single-valued integer function $h(x)$ of the x -coordinate, with steps $\delta(x) = h(x + 1/2) - h(x - 1/2)$ at integer values of x . A typical SOS interface configuration is shown in Fig. 1. The heights of the individual steps are assumed to be statistically independent and, in the case of a flat interface, identically distributed. These assumptions are exact in equilibrium [16]. The step-height probability density function (PDF) is given by the interaction energy corresponding to the $|\delta(x)|$ broken J_x -bonds between spins in the columns centered at $(x - 1/2)$ and $(x + 1/2)$ as

$$p[\delta(x)] = Z(\phi)^{-1} X^{|\delta(x)|} e^{\gamma(\phi)\delta(x)}. \quad (4)$$

The Boltzmann factor $X = e^{-2\beta J_x}$ determines the width of the PDF, and the Lagrange multiplier $\gamma(\phi)$ maintains the mean step height at an x -independent value, $\langle \delta(x) \rangle = \tan \phi$, where ϕ is the overall angle between the interface and the x axis. The Lagrange multiplier is given by

$$e^{\gamma(\phi)} = \frac{(1 + X^2) \tan \phi + \left[(1 - X^2)^2 \tan^2 \phi + 4X^2 \right]^{1/2}}{2X (1 + \tan \phi)}. \quad (5)$$

The partition function for the step height $\delta(x)$ is

$$Z(\phi) = \sum_{\delta=-\infty}^{+\infty} X^{|\delta|} e^{\gamma(\phi)\delta} = \frac{1 - X^2}{1 - 2X \cosh \gamma(\phi) + X^2}. \quad (6)$$

(See details in Refs. [3, 5]). Simple results are obtained for $\phi = 0$, which yields $\gamma(0) = 0$ and

$$Z(0) = (1 + X)/(1 - X), \quad (7)$$

and for $\phi = 45^\circ$, which yields

$$e^{\gamma(45^\circ)} = (1 + X^2)/2X \quad (8)$$

and

$$Z(45^\circ) = 2(1 + X^2)/(1 - X^2). \quad (9)$$

For soft dynamics (but not for hard dynamics), X remains independent of H when the system is driven away from equilibrium [3, 4, 5].

The mean spin-class populations, $\langle n(jks) \rangle$, are all obtained from the product of the independent PDFs for $\delta(x)$ and $\delta(x+1)$. Symmetry of $p[\delta(x)]$ under the transformation $(x, \phi, \delta) \rightarrow (-x, -\phi, -\delta)$ ensures that $\langle n(jk-) \rangle = \langle n(jk+) \rangle$ for all j and k . Numerical results illustrating the breakdown of this up/down symmetry for large $|H|$ are discussed in Sec. III B. As discussed in Ref. [3], calculation of the individual class populations is straightforward but somewhat tedious, especially for nonzero ϕ . The final results are summarized in Table II.

Whenever a spin flips from -1 to $+1$, the corresponding column of the interface advances by one lattice constant in the y direction. Conversely, the column recedes by one lattice constant when a spin flips from $+1$ to -1 . The corresponding energy changes are given in the third and fourth columns of Table I. Since the spin-class populations on both sides of the interface are equal in this approximation, the contribution to the mean velocity in the y direction from sites in the classes $jk-$ and $jk+$ becomes

$$\langle v_y(jk) \rangle = W(\beta\Delta E(jk-)) - W(\beta\Delta E(jk+)) . \quad (10)$$

The results corresponding to the soft Glauber transition probabilities used here, Eq. (3), are listed in the last column of Table II. The mean propagation velocity perpendicular to the interface becomes

$$\langle v_\perp(T, H, \phi) \rangle = \cos \phi \sum_{j,k} \langle n(jks) \rangle \langle v_y(jk) \rangle , \quad (11)$$

where the sum runs over the classes included in Table II. While the general result is cumbersome if written out in detail, using the fact that $e^{-4\beta J_x} = X^2$ for the soft Glauber dynamic [3, 4, 5], we obtain relatively compact formulas for the special cases of $\phi = 0$ and $\phi = 45^\circ$:

$$\langle v_\perp(T, H, 0) \rangle = X \left\{ \frac{1}{1+X^2} + \frac{X}{(1+X)^2(1-X^2)} \left[\frac{2(1+2X)}{1+e^{4\beta J_y}} + \frac{X^2}{1+X^2 e^{4\beta J_y}} \right] \right\} \tanh(\beta H) \quad (12)$$

and

$$\langle v_\perp(T, H, 45^\circ) \rangle = \left\{ \frac{1}{2} + \frac{2X^2}{(1+X^2)^2} + \frac{1}{1-X^4} \left[\frac{1+2X^2+3X^4}{1+e^{4\beta J_y}} + \frac{X^4}{1+X^2 e^{4\beta J_y}} \right] \right\} \frac{\tanh(\beta H)}{2\sqrt{2}} . \quad (13)$$

III. COMPARISON WITH MONTE CARLO SIMULATIONS

We have compared the analytical estimates of the propagation velocities and spin-class populations developed above with MC simulations of the same model for $J_x = J_y = J$. The details of our implementation of the discrete-time

n -fold way rejection-free MC algorithm [13] are described in Ref. [3]. By keeping only the interface sites in memory, the algorithm is not subject to size limitations in the y direction, enabling simulations for arbitrarily long times.

Our numerical results are based on simulations with $L_x = 10\,000$ and ϕ between 0 and 45° for several temperatures below T_c . ($T_c = -2J/\ln(\sqrt{2} - 1) \approx 2.269J$ is the critical temperature for the isotropic, square-lattice Ising model [17].) In order to ensure stationarity we ran the simulation for $10\,000$ n -fold way updates per updatable spin (UPS) before taking any measurements, and the results were averaged over $200\,000$ UPS [18].

A. Interface velocities

First we compare the simulated interface velocities with the analytical approximation, Eq. (11). Figure 2 shows the normal velocity vs H for $\phi = 0$ and a range of temperatures up to T_c . There is excellent agreement between the MC results and the theory for temperatures below $0.8T_c$.

The dependence of the normal velocity on the tilt angle ϕ is shown in Fig. 3 for several values of H/J between 0.1 and 3.0 . At $T = 0.2T_c$ the velocity increases with ϕ in agreement with the polynuclear growth model [6, 19, 20] at small angles and the single-step model for larger angles [6, 14, 21, 22] [Fig. 3(a)]. At $T = 0.6T_c$, on the other hand, the velocity is nearly isotropic, with a weak increase with ϕ for the strongest fields [Fig. 3(b)]. For the lowest temperature the agreement between the simulations and the analytical results is excellent everywhere. For the higher temperature it is also reasonable, but better for weak than for strong fields.

The temperature dependence of the normal interface velocity is shown in Fig. 4 for several values of H/J between 0.1 and 3.0 . The agreement between the simulations and the analytical results is excellent except for combinations of high temperatures and strong fields. In contrast to the results for hard dynamics (see Fig. 5 of Ref. [3] for Ising interfaces and Fig. 8 of Ref. [5] for SOS interfaces), the velocity goes to zero at $T = 0$ for *all* values of H , not just for $H/J < 2$. This result agrees with our finding for the SOS model with soft dynamics [4]. As predicted by the theoretical results in Ref. [3], there is thus *no* discontinuity in the interface velocity at $T = 0$ and $H/J = 2$ for soft dynamics.

B. Spin-class populations and skewness

A closer look at the performance of the mean-field approximation for the interface structure is provided by the mean spin-class populations. The analytical predictions for the class populations are based on the assumption that

different steps are statistically independent. A comparison of the simulation results with the analytical predictions therefore gives a way of testing this assumption.

The ten mean class populations that have nonzero populations in the SOS approximation, $\langle n(01s) \rangle$, $\langle n(11s) \rangle$, $\langle n(10s) \rangle$, and $\langle n(21s) \rangle$, and $\langle n(20s) \rangle$ with $s = \pm 1$ are shown vs H in Fig. 5(a) for $\phi = 0$ and $T = 0.6T_c$. Filled symbols represent $s = +1$, while empty symbols (almost completely hidden behind the corresponding filled symbols) represent $s = -1$. The class populations are practically independent of H , in agreement with the theoretical prediction for the soft dynamic [3, 4], and in contrast to the result for the Ising model with hard Glauber dynamics (see Fig. 7(a) of Ref. [3]). Deviations from the SOS approximation are indicated by the nonzero populations in the classes with two broken y -bonds, $\langle n(12s) \rangle$, $\langle n(22s) \rangle$, and $\langle n(02s) \rangle$, which are shown in Fig. 5(b). These populations are only of the order of 10^{-3} , about two orders of magnitude less than for the hard Glauber dynamic (see Fig. 7(b) of Ref. [3]), and they show significant differences between the two spin values (see below). Figure 5(c) shows the combined populations in classes with one, two, three, and four broken bonds, respectively. The results are dominated by the SOS-compatible classes and show good agreement between simulations and theory.

The skewness between the spin populations on the leading and trailing edges of the interface are a consequence of short-range correlations between neighboring steps, and it is quite commonly observed in driven interfaces. This is the case, even when the *long-range* correlations vanish as they do for interfaces in the KPZ dynamic universality class [1, 23], to which the present model belongs. Skewness has also been observed in several other SOS-type models [24, 25, 26]. The correlations associated with the skewness generally lead to a broadening of protrusions on the leading edge (“hilltops”), while those on the trailing edge (“valley bottoms”) are sharpened [24], or the other way around [26]. In terms of spin-class populations, the former corresponds to $\langle n(21-) \rangle > \langle n(21+) \rangle$ and $\langle n(11+) \rangle > \langle n(11-) \rangle$. The relative skewness can therefore be quantified by the two functions,

$$\rho = \frac{\langle n(21-) \rangle - \langle n(21+) \rangle}{\langle n(21-) \rangle + \langle n(21+) \rangle}, \quad (14)$$

introduced by Neergaard and den Nijs [24], and

$$\epsilon = \frac{\langle n(11+) \rangle - \langle n(11-) \rangle}{\langle n(11+) \rangle + \langle n(11-) \rangle}. \quad (15)$$

These two skewness parameters for the current system are shown together versus H in Fig. 6(a). The skewness is very weak, but it is not zero in contrast to the SOS model with soft Glauber dynamic [4]. Both these skewness parameters have the opposite sign and are about two orders of magnitude smaller than in the Ising model with the hard Glauber dynamic [3] [Fig. 6(b)] and in the SOS model with the same hard dynamic [5] [Fig. 6(c)].

The skewness parameters ρ and ϵ depend on spin classes which have nonzero populations in the SOS picture, and they can therefore be applied to both Ising and SOS interfaces. In the Ising case, however, much more pronounced differences are seen in the populations of those classes that are not populated in the SOS model [see Fig. 5(b)]. For Ising models, these classes can be used to define further skewness parameters, such as

$$\kappa = \frac{\langle n(22-) \rangle - \langle n(22+) \rangle}{\langle n(22-) \rangle + \langle n(22+) \rangle}. \quad (16)$$

Here class $22-$ represents isolated bubbles of the metastable phase that persist as a “wake” behind the moving interface, while $22+$ corresponds to a “bow wave” of bubbles of the stable phase in front of the interface, which are created by pinching-off of protrusions. Although the total density of such bubbles is about two orders of magnitude smaller with the soft dynamic studied here than with hard dynamics (compare Fig. 5(b) with Fig. 7(b) of Ref. [3]), the relative asymmetry parameters κ are comparable, as shown in Fig. 7. Not surprisingly, for strong fields the entire bubble population is found in the wake, yielding $\kappa \lesssim 1$ in this limit.

IV. CONCLUSION

In this paper we have continued our study of the dependence of the local structure of driven interfaces on the applied field and temperature and on the form of the stochastic dynamics under which they move [3, 4, 5]. The local interface structure is of interest because it is it, rather than the large-scale scaling behavior, which determines such important interface properties as mobility and chemical reactivity. In particular, we studied the differences between interfaces moving under *soft* stochastic dynamics, in which the influences of changes in the field energy and the interaction energy factorize in the transition probabilities, and *hard* dynamics, which do not possess such a factorization property.

We find that the results for the Ising model with the soft Glauber dynamic, which is the main topic of this study, differ relatively little from the SOS model with soft dynamics studied in Ref. [4]. In particular, the local interface width does *not* diverge with increasing H , as it does for both the Ising [3] and SOS [5] models with hard dynamics. As a result, the soft dynamics do not produce the discontinuity in the interface velocity at $H/J = 2$ and $T = 0$ that is seen for hard dynamics. The main qualitative difference between the Ising and SOS models with soft dynamics is that the interface skewness for the Ising model in nonzero field is not exactly zero, as it is for the SOS model. However, the skewness parameters ρ and ϵ , which are based on SOS-compatible spin classes, are about two orders of magnitude smaller and have the opposite sign than what is seen for the hard dynamics. In contrast, the relative asymmetry in the populations of bubbles behind and in front of the interface (which do not occur in SOS models) can be expressed

by the skewness parameter κ and is comparable for the two dynamics. However, the *absolute* bubble density is about two orders of magnitude smaller with the soft than with the hard dynamics. Although a successful mean-field theory for the interface mobility of different models and under different stochastic dynamics was developed in Refs. [3, 5], a comparable theory that predicts the skewness is still not available.

Two important conclusions can be drawn from our studies. First, the strong differences between hard and soft dynamics make it evident that great care must be used in formulating and interpreting stochastic models of dynamic systems. Second, experimental observation of the field and temperature dependences of interface mobility and local interface structure could contribute significantly to devising correct stochastic models of nonequilibrium physical phenomena.

Acknowledgments

P. A. R. appreciates the hospitality of the Department of Physics, Virginia Polytechnic Institute and State University. The research was supported in part by National Science Foundation Grant Nos. DMR-9981815, DMR-0120310, and DMR-0240078, and by Florida State University through the Center for Materials Research and Technology and the School of Computational Science and Information Technology.

-
- [1] A.-L. Barabási and H. E. Stanley, *Fractal Concepts in Surface Growth* (Cambridge University Press, Cambridge, 1995), and references therein.
 - [2] P. Meakin, *Fractals, Scaling, and Growth far from Equilibrium* (Cambridge University Press, Cambridge, 1998), and references therein.
 - [3] P. A. Rikvold and M. Kolesik, *J. Stat. Phys.* **100**, 377 (2000).
 - [4] P. A. Rikvold and M. Kolesik, *J. Phys. A: Math. Gen.* **35**, L117 (2002).
 - [5] P. A. Rikvold and M. Kolesik, *Phys. Rev. E* **66**, 066116 (2002).
 - [6] P. Devillard and H. Spohn, *Europhys. Lett.* **17**, 113 (1992).
 - [7] R. A. Ramos, P. A. Rikvold, and M. A. Novotny, *Phys. Rev. B* **59**, 9053 (1999).
 - [8] M. A. Novotny, P. A. Rikvold, M. Kolesik, D. M. Townsley, and R. A. Ramos, *J. Non-Cryst. Solids* **274**, 356 (2000).
 - [9] D. P. Landau and K. Binder *Monte Carlo Simulations in Statistical Physics* (Cambridge Univ. Press, Cambridge, 2000).
 - [10] J. Marro and R. Dickman, *Nonequilibrium Phase Transitions in Lattice Models* (Cambridge University Press, Cambridge, 1999), Ch. 7.

- [11] H. Guo, B. Grossmann, and M. Grant, *Phys. Rev. Lett.* **64**, 1262 (1990).
- [12] M. Kotrla and A. C. Levi, *J. Stat. Phys.* **64**, 579 (1991).
- [13] A. B. Bortz, M. H. Kalos, and J. L. Lebowitz, *J. Comput. Phys.* **17**, 10 (1975).
- [14] H. Spohn, *J. Stat. Phys.* **71**, 1081 (1993).
- [15] M. A. Novotny, *Computers in Physics* **9**, 46 (1995).
- [16] W. K. Burton, N. Cabrera, and F. C. Frank, *Phil. Trans. Roy. Soc. (London) Ser. A* **243**, 299 (1951).
- [17] L. Onsager, *Phys. Rev.* **65**, 117 (1944).
- [18] Each simulation run for a specific set of values of all parameters took about 80 minutes on an AMD Athlon PC running Linux.
- [19] J. Krug and H. Spohn, *Europhys. Lett.* **8**, 219 (1989).
- [20] J. Kertész and D. E. Wolf, *Phys. Rev. Lett.* **62**, 2571 (1989).
- [21] P. Meakin, P. Ramanlal, L. M. Sander, and R. C. Ball, *Phys. Rev. A* **34**, 5091 (1986).
- [22] M. Plischke, Z. Rácz, and D. Liu, *Phys. Rev. B* **35**, 3485 (1987).
- [23] M. Kardar, G. Parisi, and Y.-C. Zhang, *Phys. Rev. Lett.* **56**, 889 (1986).
- [24] J. Neergaard and M. den Nijs, *J. Phys. A: Math. Gen.* **30**, 1935 (1997).
- [25] O. Pierre-Louis, M. R. D'Orsogna, and T. L. Einstein, *Phys. Rev. Lett.* **82**, 3661 (1999).
- [26] G. Korniss, Z. Toroczkai, M. A. Novotny, and P. A. Rikvold, *Phys. Rev. Lett.* **84**, 1351 (2000).

TABLE I: The spin classes in the anisotropic square-lattice Ising model. First column: the class labels, jks . Second column: the total energy per spin, $E(jks)$, relative to the state with all spins parallel and $H = 0$, $E_0 = -2(J_x + J_y)$. Third column: the change in the field energy resulting from spin reversal from s to $-s$, $\Delta E_H(jks)$. Fourth column: the corresponding change in the interaction energy, $\Delta E_J(jks)$. In columns two and three, the upper (lower) sign corresponds to $s = -1$ ($s = +1$). The first three classes have nonzero populations in the SOS approximation, and flipping a spin in any of them preserves the SOS configuration. The two classes marked † also have nonzero populations in the SOS approximation, but flipping a spin in any of them may produce an overhang or a bubble. The two classes marked ‡ are not populated in the SOS approximation, but flipping a spin in any of them may produce an SOS configuration. The two classes marked * correspond to a bulk spin that is either parallel or antiparallel to all its neighbors. Flipping a spin in class $22s$ yields a spin in class $00-s$. The transition probabilities for all classes except $00s$ (from which transitions are forbidden with the dynamic used here) are given by Eq. (3).

Class, jks	$E(jks) - E_0$	$\Delta E_H(jks)$	$\Delta E_J(jks)$
$01s$	$\pm H + 2J_y$	$\mp 2H$	$+4J_x$
$11s$	$\pm H + 2(J_x + J_y)$	$\mp 2H$	0
$21s$	$\pm H + 2(2J_x + J_y)$	$\mp 2H$	$-4J_x$
$10s$ †	$\pm H + 2J_x$	$\mp 2H$	$+4J_y$
$20s$ †	$\pm H + 4J_x$	$\mp 2H$	$-4(J_x - J_y)$
$12s$ ‡	$\pm H + 2(J_x + 2J_y)$	$\mp 2H$	$-4J_y$
$02s$ ‡	$\pm H + 4J_y$	$\mp 2H$	$+4(J_x - J_y)$
$22s$ *	$\pm H + 4(J_x + J_y)$	$\mp 2H$	$-4(J_x + J_y)$
$00s$ *	$\pm H$	$\mp 2H$	$+4(J_x + J_y)$

TABLE II: The mean populations for the spin classes that have nonzero populations in the SOS approximation, with the corresponding contributions to the interface velocity under the soft Glauber dynamic. First column: the class labels, jks . Second column: the mean spin-class populations for general tilt angle ϕ , with $\cosh \gamma(\phi)$ from Eq. (5). Third and fourth columns: the spin-class populations for $\phi = 0$ [using $\gamma(0) = 0$] and $\phi = 45^\circ$ [using Eq. (8) for $\exp[\gamma(45^\circ)]$], respectively. Fifth column: the contributions to the mean interface velocity in the y direction from spins in classes $jk-$ and $jk+$, Eq. (10), using the soft Glauber dynamic, Eq. (3).

Class, jks	$\langle n(jks) \rangle$, general ϕ	$\langle n(jks) \rangle$, $\phi = 0$	$\langle n(jks) \rangle$, $\phi = 45^\circ$	$\langle v_y(jk) \rangle$
01s	$\frac{1-2X \cosh \gamma(\phi)+X^2}{(1-X^2)^2}$	$\frac{1}{(1+X)^2}$	$\frac{1}{2(1+X^2)}$	$\frac{\tanh(\beta H)}{1+e^{4\beta J_x}}$
11s	$\frac{2X[(1+X^2) \cosh \gamma(\phi)-2X]}{(1-X^2)^2}$	$\frac{2X}{(1+X)^2}$	$\frac{1}{2}$	$\frac{\tanh(\beta H)}{2}$
21s	$\frac{X^2[1-2X \cosh \gamma(\phi)+X^2]}{(1-X^2)^2}$	$\frac{X^2}{(1+X)^2}$	$\frac{X^2}{2(1+X^2)}$	$\frac{\tanh(\beta H)}{1+e^{-4\beta J_x}}$
10s †	$\frac{2X^2}{1-X^2} \left\{ \frac{2 \cosh^2 \gamma(\phi)-1-2X \cosh \gamma(\phi)+X^2}{1-2X \cosh \gamma(\phi)+X^2} - \frac{X^2[1-2X \cosh \gamma(\phi)+X^2]}{(1-X^2)^2} \right\}$	$\frac{2X^2(1+2X)}{(1-X^2)(1+X)^2}$	$\frac{1+2X^2+3X^4}{2(1-X^4)}$	$\frac{\tanh(\beta H)}{1+e^{4\beta J_y}}$
20s †	$\frac{X^4[1-2X \cosh \gamma(\phi)+X^2]}{(1-X^2)^3}$	$\frac{X^4}{(1-X^2)(1+X)^2}$	$\frac{X^4}{2(1-X^4)}$	$\frac{\tanh(\beta H)}{1+e^{-4\beta(J_x-J_y)}}$

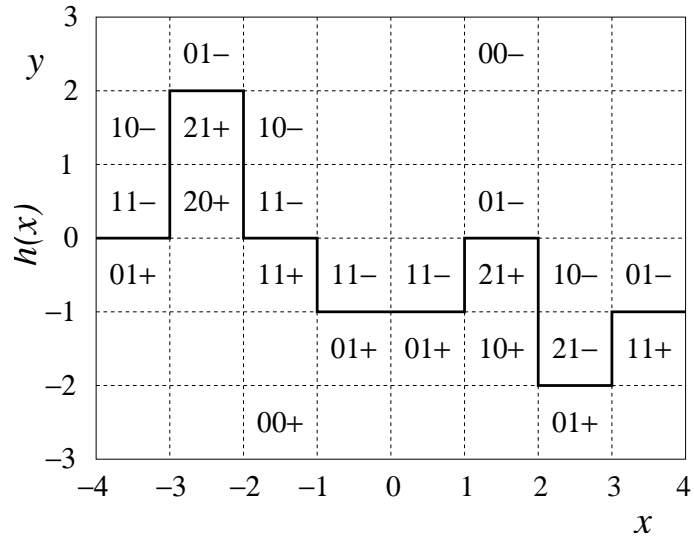


FIG. 1: A short segment of an SOS interface $y = h(x)$ between a positively magnetized phase below and a negative phase above. The step heights are $\delta(x) = h(x + 1/2) - h(x - 1/2)$. Interface sites representative of the different SOS spin classes (see Table I and Table II) are marked with the notation jks explained in the text. Sites in the uniform bulk phases are $00-$ and $00+$. From Ref. [5].

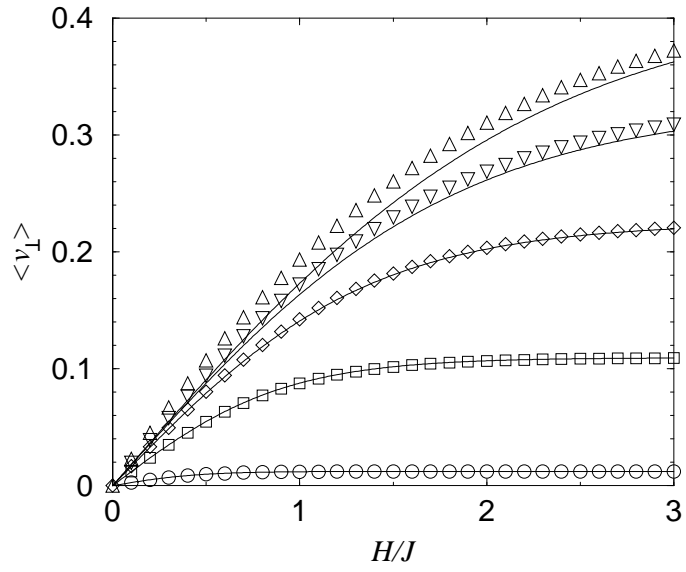


FIG. 2: The average stationary normal interface velocity $\langle v_{\perp} \rangle$, shown vs H for $\phi = 0$. The MC results are shown as data points, and the theoretical predictions as solid curves. From below to above, the temperatures are $T/T_c = 0.2, 0.4, 0.6, 0.8,$ and 1.0 .

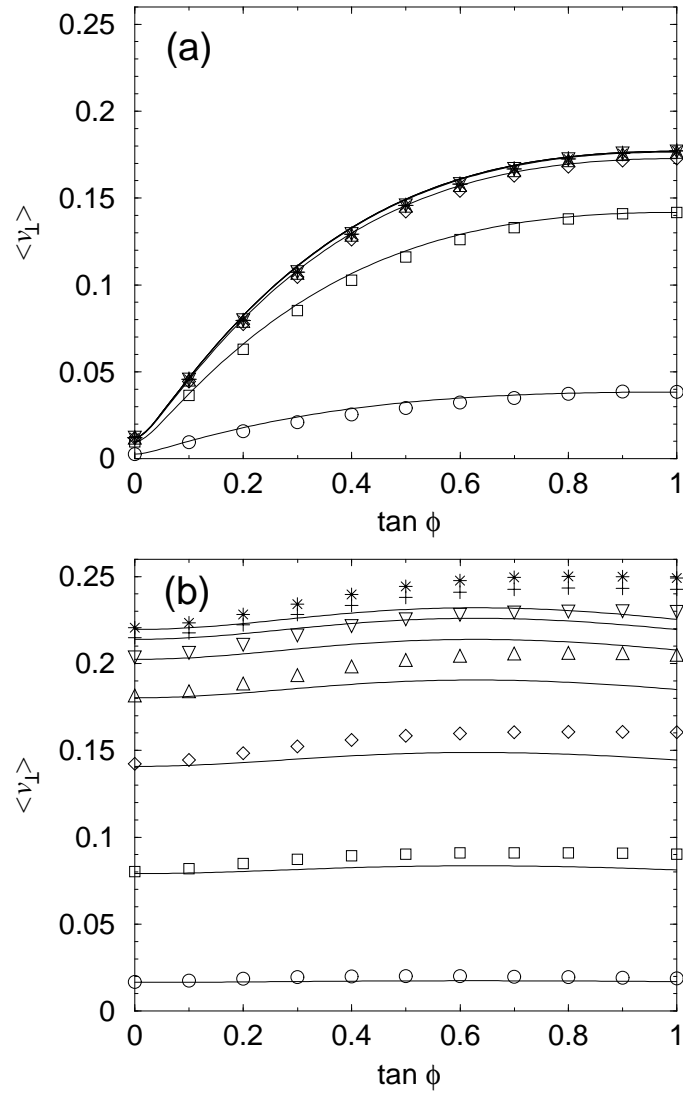


FIG. 3: The average stationary normal interface velocity $\langle v_{\perp} \rangle$, shown vs $\tan \phi$ for (from below to above) $H/J = 0.1, 0.5, 1.0, 1.5, 2.0, 2.5,$ and 3.0 . The MC results are shown as data points, and the theoretical predictions as solid curves. (a) $T = 0.2T_c$. (b) $T = 0.6T_c$.

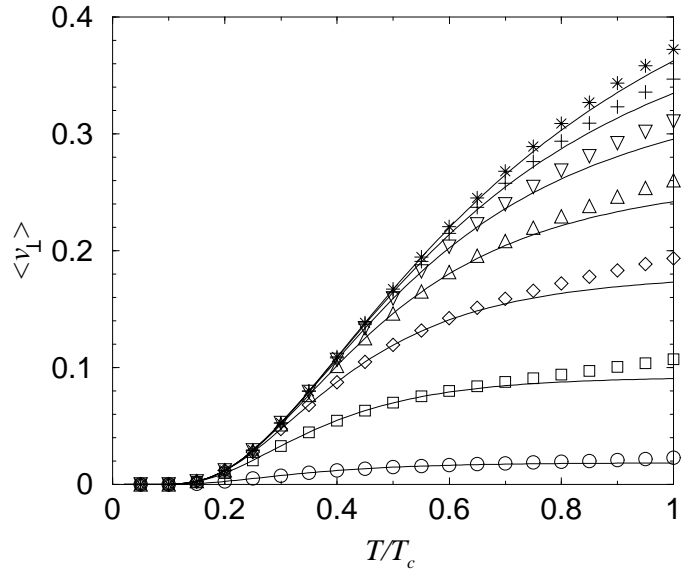


FIG. 4: The average stationary normal interface velocity $\langle v_{\perp} \rangle$, shown vs T at $\phi = 0$ for (from below to above) $H/J = 0.1, 0.5, 1.0, 1.5, 2.0, 2.5,$ and 3.0 . The MC results are shown as data points, and the theoretical predictions as solid curves.

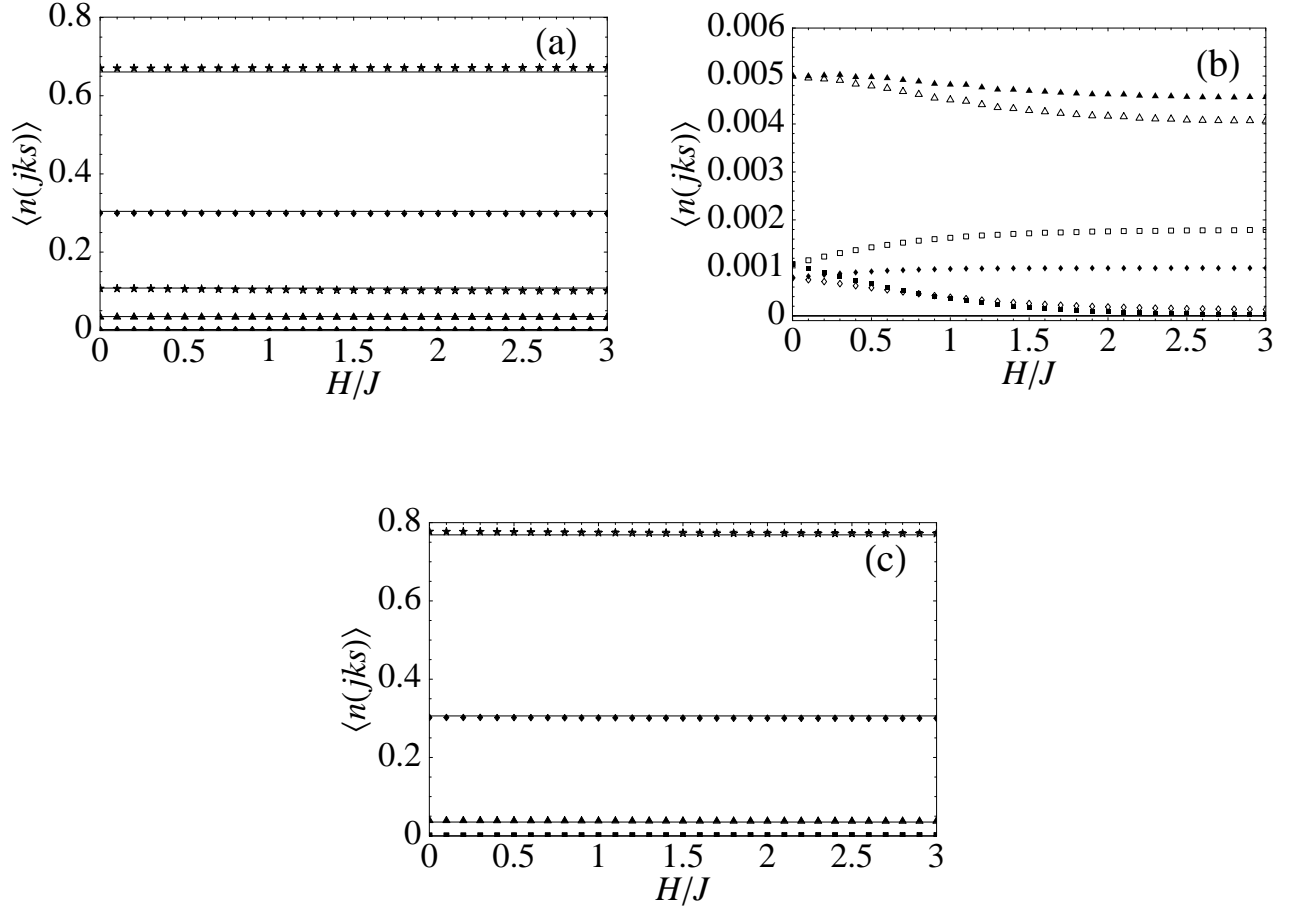


FIG. 5: Mean stationary class populations $\langle n(jks) \rangle$, shown vs H at $\phi = 0$ and $T = 0.6T_c$. Solid lines correspond to the theoretical predictions, while filled symbols denote $s = +1$ and empty symbols (in most cases hidden by the corresponding filled symbols) denote $s = -1$. (a) The ten SOS-compatible classes, from top to bottom $01s$, $11s$, $10s$, $21s$, and $20s$. (b) The six classes with two broken y -bonds, which have zero populations in the SOS approximation, $12s$ (triangles), $22s$ (squares), and $02s$ (diamonds). (c) From above to below are shown the aggregate populations of classes with one ($01s$ and $10s$), two ($11s$, $20s$, and $02s$), three ($21s$ and $12s$) and four ($22s$) broken bonds.

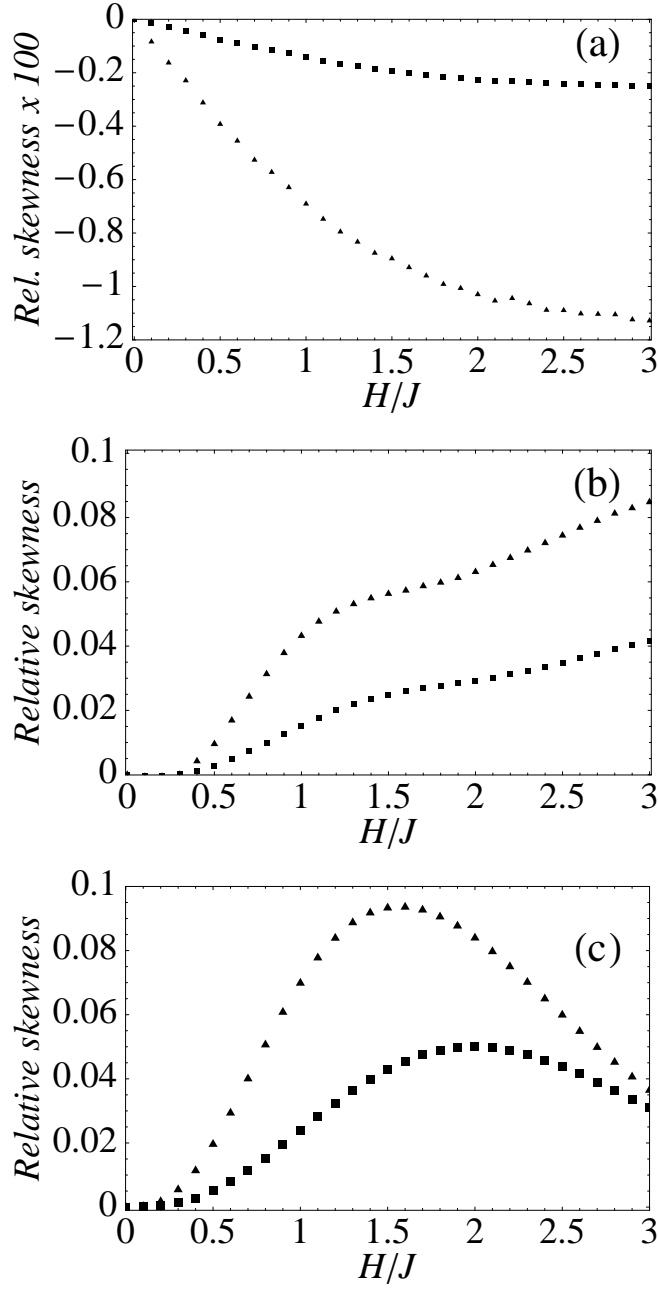


FIG. 6: The two relative skewness parameters ρ (triangles) and ϵ (squares), defined in Eqs. (14) and (15), respectively, shown vs H for $\phi = 0$ at $T = 0.6T_c$. (a) The skewness parameters multiplied by 100 for the Ising model with soft Glauber dynamics, discussed in this paper. (b) The skewness parameters (no multiplication) for the Ising model with hard Glauber dynamics, discussed in Ref. [3]. (c) The skewness parameters (no multiplication) for the SOS model with hard Glauber dynamics, from Ref. [5]. Note the different sign and the scale difference of two orders of magnitude between the soft dynamic shown in (a) and the hard dynamics shown in (b) and (c).

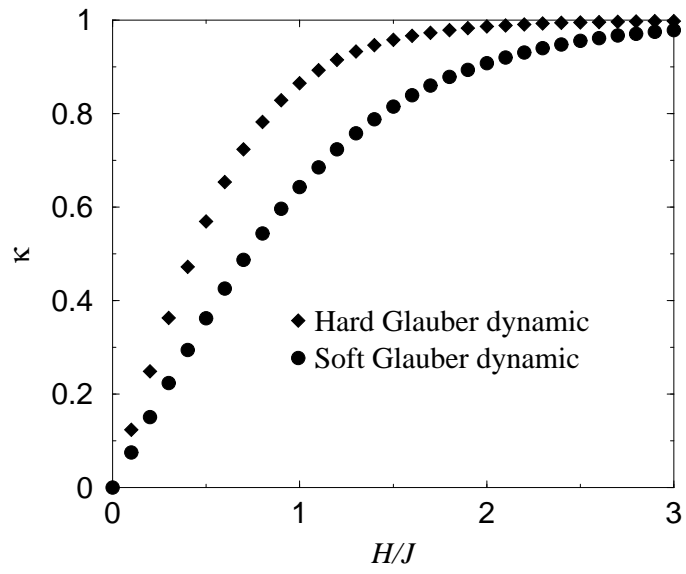


FIG. 7: The relative skewness parameter κ , shown vs H for $\phi = 0$ at $T = 0.6T_c$. It measures the asymmetry between the populations of bubbles behind and in front of the Ising interface.